Tellus SERIES B CHEMICAL AND PHYSICAL METEOROLOGY
PUBLISHED BY THE INTERNATIONAL METEOROLOGICAL INSTITUTE IN STOCKHOLM

Impacts of additional HONO sources on O_3 and $PM_{2.5}$ chemical coupling and control strategies in the Beijing–Tianjin–Hebei region of China

By YING LI[1†], JUNLING AN[1]*, MIZUO KAJINO[2,3], ISMAIL GULTEPE[4], YONG CHEN[1], TAO SONG[1] and JINYUAN XIN[1], [1]*State Key Laboratory of Atmospheric Boundary Layer Physics and Atmospheric Chemistry (LAPC), Institute of Atmospheric Physics, Chinese Academy of Sciences, Beijing, China;* [2]*Meteorological Research Institute, 1-1 Nagamine, Tsukuba, Japan;* [3]*RIKEN Advanced Institute for Computational Science, 7-1-26 Minatojima-minamimachi, Chuo-ku, Kobe, Hyogo, Japan;* [4]*Cloud Physics and Severe Weather Research Section, Environment Canada, Toronto, ON, Canada*

(Manuscript received 27 January 2014; in final form 1 February 2015)

ABSTRACT

The objective of this work is to examine the impacts of additional HONO sources on the chemical interaction between ozone (O_3) and particulate matter with a diameter ≤ 2.5 μm ($PM_{2.5}$). Three additional HONO sources, i.e. HONO emissions, the reaction of photo-excited nitrogen dioxide (NO_2^*) with water vapour (H_2O), and NO_2 heterogeneous reaction on aerosol surfaces, were inserted into the fully coupled Weather Research and Forecasting-Chemistry model to evaluate O_3 and $PM_{2.5}$ concentration enhancements in the Beijing–Tianjin–Hebei (BTH) region during August 2007. Results show that the additional HONO sources significantly increase O_3 and $PM_{2.5}$ concentrations during daytime. Up to 9 ppb enhancements of O_3 and 32 μg m^{-3} increases in $PM_{2.5}$ are found at seven urban sites over the BTH region. O_3 increases are closely connected to $PM_{2.5}$ increases over urban areas during daytime when the additional HONO sources are taken into account. $PM_{2.5}$ inorganic components of SO_4^{2-}, NO_3^- and NH_4^+ are increased by 5–18, 10–58 and 10–40%, respectively, over urban areas during daytime. The simultaneous increment of O_3 and $PM_{2.5}$ during daytime due to the additional HONO sources is related to the increasing oxidants (OH, H_2O_2 and O_3) that enhance the atmospheric oxidising capacity. The concentration variations of O_3 and $PM_{2.5}$ under a variety of NO_x, volatile organic compound and ammonia (NH_3) emission control scenarios show that the additional HONO sources increase the sensitivity of O_3 and $PM_{2.5}$ concentrations to the changes of NO_x emissions. An increase of the $PM_{2.5}$ sensitivity to changes in NH_3 emissions is also found. This indicates that without considering the additional HONO sources, the effectiveness of emission control strategies in reducing O_3 and $PM_{2.5}$ concentrations would be significantly underestimated.

Keywords: HONO sources, O_3 and $PM_{2.5}$ chemical coupling, control strategy, WRF-Chem model

To access the supplementary material to this article, please see Supplementary files under 'Article Tools'.

1. Introduction

Nitrous acid (HONO) plays an important role in enhancing O_3 and particulate matter (PM) concentrations in the polluted atmospheric boundary layer due to its photolysis into the hydroxyl radical (OH), which is a primary daytime oxidant (Alicke et al., 2002; Kleffmann et al., 2005). Jenkin et al. (2008) showed that increasing HONO emissions by 5% resulted in O_3 enhancements of 11 ppb in the southern UK during a heat-wave period of August 2003. Besides direct emissions, HONO can also be formed through gas-phase or heterogeneous reactions. The homogeneous gas-phase reaction between excited nitrogen dioxide (NO_2^*) and H_2O ($NO_2^* + H_2O \rightarrow HONO + OH$, hereafter referred to as NO_2^* chemistry) has gained interest since its reaction rate

*Corresponding author.
email: anjl@mail.iap.ac.cn
Responsible Editor: Kaarle Hämeri, University of Helsinki, Finland.
†Now at: Multiphase Chemistry Department, Max Planck Institute for Chemistry, Mainz 55128, Germany.

Citation: Tellus B 2015, **67**, 23930, http://dx.doi.org/10.3402/tellusb.v67.23930

has been found at an order of magnitude faster than the previously estimated upper limit (Crowley and Carl, 1997), thus can substantially enhance OH production (Li et al., 2008). However, the atmospheric significance of this new mechanism is highly controversial. Carr et al. (2009) argued that the NO_2^* chemistry would not be important under normal atmospheric conditions and they estimated the reaction rate similar to the result of Crowley and Carl (1997) (1.2×10^{-14} cm^3 molecule^{-1} s^{-1}). Amedro et al. (2011) claimed that no OH radicals were observed using an unfocused excitation laser beam at 565 nm, but OH formation was observed by focusing the laser beam. Recently, Wu and Chen (2012) concluded that the reaction of two photon absorbed NO_2 with H_2O makes negligible contributions to the formation of OH radicals while single photon absorption at <554 nm is a possible process.

The uncertainties in the NO_2^* chemistry did not prevent the evaluation of its potential impact on tropospheric air quality using chemical transport models. Simulations conducted in the South Coast Air Basin of California during the summer of 1987 showed that the NO_2^* chemistry increased O_3 and $PM_{2.5}$ (PM with a diameter ≤ 2.5 μm) concentrations by as much as 55 ppb and 20 μg m^{-3}, respectively (Wennberg and Dabdub, 2008). However, due to the lower ambient NO_x and volatile organic compound (VOC) levels, the impact of the NO_2^* chemistry on O_3 enhancement was found to be smaller in the U.S. after the year of 2000. The maximum increases of O_3 concentrations in urban areas in the U.S. less than 10 ppb (Sarwar et al., 2009; Ensberg et al., 2010) suggest that the effect of the NO_2^* chemistry on pollution levels may be more significant in some industrialised regions with elevated levels of ambient NO_x and VOCs, such as mega-cities in China. Thereafter studies reported that O_3 enhancements were more than 30 ppb in Beijing (Li et al., 2011) and Taiwan (Jorba et al., 2012), and 10 ppb over the urban areas of the Pearl River Delta region of China (Zhang et al., 2013).

Along with the direct emissions and the homogeneous formation of HONO, NO_2 heterogeneous reaction on wet surfaces ($2NO_2 + H_2O \rightarrow HNO_3 + HONO$) is commonly considered as one of the major HONO heterogeneous sources (Jenkin et al., 1988; Kleffmann et al., 1998; Finlayson-Pitts et al., 2003). The NO_2 heterogeneous reaction has been included previously in the Community Multiscale Air Quality (CMAQ) modelling system (Foley et al., 2010). The CMAQ simulations showed that the NO_2 heterogeneous reaction was found to be the most significant source of nocturnal HONO formation during the project of the Northeast Oxidant and Particle Study in the U.S. (Sarwar et al., 2008). The simulations conducted over the Beijing–Tianjin–Hebei region (referred as BTH region), as the most polluted areas in China, suggested that the largest enhancements of the monthly mean daytime O_3 and $PM_{2.5}$ during August 2007 were about 12 and 16%, respectively, and this was mostly due to the NO_2 heterogeneous reaction on aerosol surfaces (An et al., 2013).

In addition to direct emissions, homogeneous gas-phase formation and heterogeneous reactions, a recent study has demonstrated that ammonia-oxidising bacteria in soil can directly release HONO (Oswald et al., 2013). The soil HONO emissions may play an important role in the biogeochemical and atmospheric nitrogen cycles. This finding helps understand how the biosphere affects the atmosphere and global climate. Before this new mechanism can be incorporated into chemical transport models, continuous and comprehensive field measurements are needed, including simultaneous monitoring of soil, ecosystem and atmospheric processes.

Previous studies mainly focused on the impacts of HONO sources on O_3 and $PM_{2.5}$ concentrations but rarely considered the relationship between O_3 and $PM_{2.5}$ enhancements due to HONO sources. Meng et al. (1997) pointed out that there was a complex chemical coupling between O_3 and $PM_{2.5}$ components because they shared the same precursors as NO_x and VOCs. In-situ observations also proved that severe PM pollution was often accompanied with high O_3 concentrations. Positive correlation between the daily $PM_{2.5}$ and maximum 8-h O_3 ($O_{3\_8h;max}$) concentrations was also observed over the BTH region during the Beijing 2008 Olympic Games (Xin et al., 2010). When additional HONO sources were considered in the O_3 and $PM_{2.5}$ interaction, another level of complexity was added into the chemical coupling system (Wennberg and Dabdub, 2008) and this impacted O_3 and $PM_{2.5}$ emission control strategies (Meng et al., 1997). Ensberg et al. (2010) studied the impacts of the NO_2^* chemistry on O_3 and PM control strategies over the South Coast Air Basin of California during two emission episodes that occurred for 1987 and 2005. They showed that the NO_2^* chemistry increased the sensitivity of O_3 and secondary PM concentrations with respect to changes in NO_x emissions (Ensberg et al., 2010). Notable changes in O_3 responses to NO_x and VOC emission controls were also found in the Pearl River Delta of China due to the NO_2^* chemistry (Zhang et al., 2013). These studies suggested that the additional HONO sources had significant implications for polluted areas to achieve ozone and PM air quality standards.

In spite of considerable improvements in air quality indexes over the last decade, the BTH region continues to suffer from severe O_3 and PM pollution as well as haze (Chan and Yao, 2008; Sun et al., 2013; Zhao et al., 2013). Significant O_3 and $PM_{2.5}$ enhancements over the BTH region during August 2007 due to three additional HONO sources (including HONO emissions, the NO_2^* chemistry and NO_2 heterogeneous reaction on aerosol surfaces) were also reported by Li et al. (2011) and An et al. (2013).

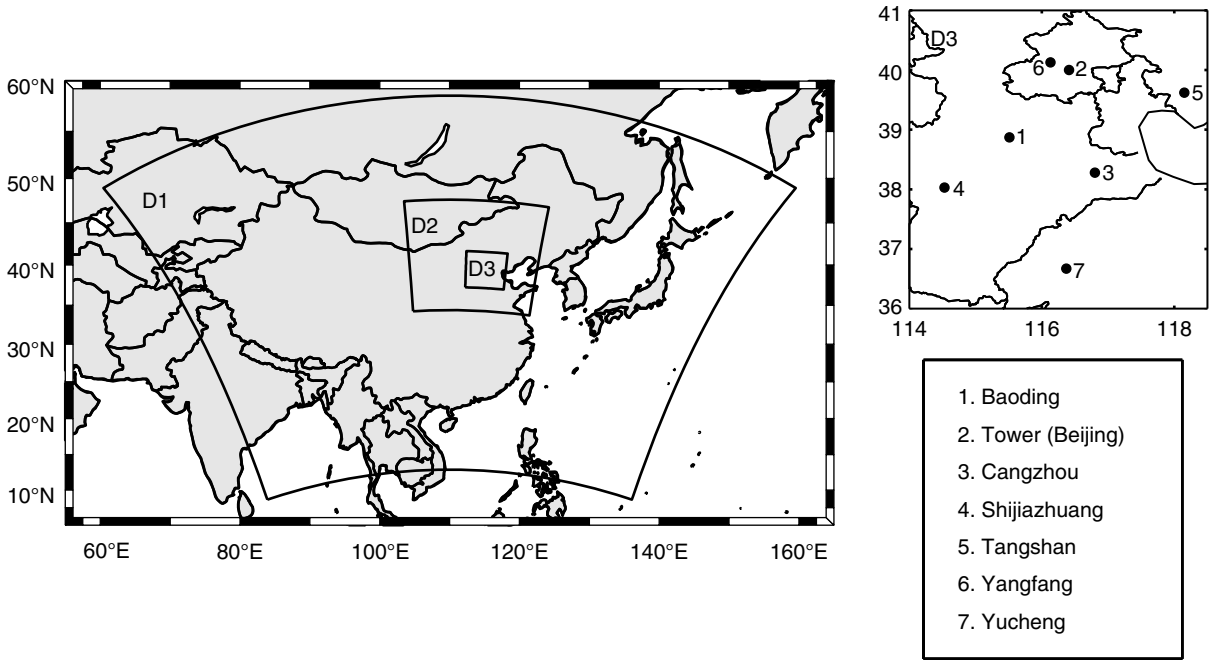

Fig. 1. Modelling domains and the monitoring sites over the BTH region.

These works suggested that more strict conditions on O_3 and PM concentration standards were needed to be set up. Presently, the China's Grade-2 Standard list[1] includes the daily $O_{3\_8h;max}$ at 160 μg m^{-3} and 24-h average $PM_{2.5}$ at 75 μg m^{-3}.

There are two main objectives in this study: (1) to analyse the relationship between the enhancements of daytime O_3 and $PM_{2.5}$ as a function of the additional HONO sources and (2) examine the reductions of daily $O_{3\_8h;max}$ and 24-h averaged $PM_{2.5}$ concentrations as functions of NO_x, VOC and NH_3 emission reductions when the additional HONO sources are considered. Section 2 is introduced for the numerical experiments conducted in this study. Section 3 describes observation data used in the model evaluation. The effects of the additional HONO sources on O_3 and $PM_{2.5}$ chemical coupling and control strategies are discussed in Section 4 and the conclusions are presented in Section 5.

2. Model description

2.1. WRF-Chem model and new parameterisation of HONO

This study utilised a fully coupled Weather Research and Forecasting-Chemistry (WRF-Chem) model (Grell et al., 2005; Fast et al., 2006) with the gas phase chemical Carbon-Bond Mechanism Z (CBM-Z; Zaveri and Peters, 1999) and aerosol module of the Model for Simulating Aerosol Interactions and Chemistry (MOSAIC; Zaveri et al., 2008). The physical schemes for simulations were identical to those chosen by Li et al. (2011).

Figure 1 shows the domains of the simulations. Domain 1, 2 and 3 primarily cover the Eastern Asia, Northern China and BTH region, respectively. Domain 3 contains 54×54 grids with a grid resolution of 9 km and centres at 40°N, 116°E. The 28 vertical layers extend from the surface to 50 hPa with the first level at 28 m above the ground. Meteorological initial and boundary conditions were obtained from the US National Centers for Environmental Prediction (NCEP; 6-h, $1^\circ \times 1^\circ$) final operation global analysis dataset. Chemical initial and boundary conditions were interpolated from the Model for OZone And Related chemical Tracers version 4 (MOZART-4; Emmons et al., 2010) outputs at every 6 h. Monthly anthropogenic emissions covering East Asia with a grid resolution of $0.5^\circ \times 0.5^\circ$ were adopted from Zhang et al. (2009). Future emission inventory over this region requires a finer grid resolution to help air quality models better capture the localised photochemistry in the atmosphere. Biogenic emissions were calculated based on Guenther et al. (1993) and Simpson et al. (1995).

The following input for model reference simulation and test runs was considered. Besides HONO gas-phase production from OH and NO, three additional HONO sources

[1]http://kjs.mep.gov.cn/hjbhbz/bzwb/dqhjbh/dqhjzlbz/201203/W020120410330232398521.pdf

(i.e. HONO emissions, the NO_2^* chemistry and NO_2 heterogeneous reaction on aerosol surfaces) were coupled into the WRF-Chem model. Li et al. (2011, 2014) and An et al. (2013) have described the parameterisation schemes in detail. Briefly, HONO emissions included direct emissions estimated as 0.8% of NO_x emissions (Kurtenbach et al., 2001) and 2.3% of the NO_x emitted in diesel exhaust gases converted to HONO via heterogeneous reaction with semi-volatile organics (Gutzwiller et al., 2002). The ratio of $HONO/NO_x$ used in the model set up was about 1.18% in the urban centre of Beijing (Li et al., 2011; An et al., 2013). The rate constant for the reaction of NO_2^* with H_2O was estimated as 9.1×10^{-14} cm^3 molecule^{-1} s^{-1} which was similar to the mean values of Li et al. (2008) and Crowley and Carl (1997). The NO_2 heterogeneous reaction on aerosol surfaces followed Jacob (2000) recommendations. To compute the reaction rate, the total aerosol surface area (S_a) per unit volume of air is derived from aerosol mass concentrations and number density in eight size bins set by the MOSAIC aerosol module. The mean calculated S_a was 1367 μm^2 cm^{-3} in Beijing during August 2007, within the observed range of 1000–2500 μm^2 cm^{-3} (Spataro et al., 2013).

2.2. Experimental design

Five simulations given in Table 1 were conducted in this study. The first one was a reference case (Case R) that was performed using the standard CBM-Z mechanism and the MOSAIC module. Case Emis, Case NO_2^* and Case Het were extensions of Case R by inclusion of HONO emissions, the NO_2^* chemistry and the NO_2 heterogeneous reaction, respectively. The last simulation referred as an enhanced case (Case E) contained all the three additional HONO sources. The simulation period was August 2007, during which an extensive observed dataset was obtained, including highly time-resolved ambient gas phase species and aerosols (shown in Section 3).

Table 1. Design of WRF–Chem simulations to evaluate the effects of the additional HONO sources

Case ID	HONO sources included in the WRF–Chem simulations
Case R	Reference case with HONO gas-phase production from OH and NO
Case Emis	Case R + HONO emissions
Case NO_2^*	Case R + NO_2^* chemistry
Case Het	Case R + NO_2 heterogeneous reaction on aerosol surfaces
Case E	Enhanced case with all the three additional HONO sources

Additional sensitivity runs for the impacts of the three additional HONO sources on O_3 and $PM_{2.5}$ control strategies were conducted on 17 August 2007 when the BTH region experienced exceedingly high ozone and PM levels. The daily $O_{3\_8h;max}$ in Beijing violated China's Grade-2 Standard values. In order to save the computational time, four emission scaling factors, i.e. 1, 0.75, 0.5 and 0.25, are employed. The reference case emissions (Zhang et al., 2009) of NO_x, VOCs and NH_3 were multiplied by the scaling factors individually, leading to 64 emission scenarios. The 128 (64×2) sensitivity simulations were conducted for Domain 3. The first 64 scenarios employed the standard CBM-Z and MOSAIC modules and the remaining 64 scenarios included the three additional HONO sources. All of the simulations started with the initial conditions at 00:00/16/8/2007 (UTC) using the standard CBM-Z and MOSAIC modules for the reference case emissions, then they were integrated from 00:00/16/8/2007 to 00:00/18/8/2007 (UTC) under different emission scenarios.

3. Observations and data

The HONO concentrations were measured on a 24-h basis by the annular denuder system at the campus of Peking University (39.99°N, 116.28°E) from 2 to 31 August 2007 as part of the CAREBeijing-2007 Experiment (2007 Campaigns of Air Quality Research in Beijing; Spataro et al., 2013). Measurements of NO_2, nitrate (NO_3^-) and ammonium (NH_4^+) were also used in this study (Ianniello et al., 2011). Hourly HONO concentrations were taken from Differential Optical Absorption Spectroscopy (DOAS) measurements in Beijing from 13 to 25 August 2007 (Zhu et al., 2009). The retroreflector array was placed on a platform at 15 m of the 325 m Meteorological Tower located at the Institute of Atmospheric Physics (IAP; 39.97°N, 116.37°E). The fixed light path was 470 m (one way) across an expressway (Li et al., 2011). Hourly measurements of meteorological parameters including air temperature (T), relative humidity (RH), wind speed (WS) and direction (WD) from 13 to 20 August were adopted from the Olympic Village (40.00°N, 116.37°E) site close to IAP because the observed meteorological data at the tower site were unavailable within the studied period. There was no precipitation happening during this period. Observations of the surface NO_2, O_3 and $PM_{2.5}$ concentrations over the BTH region were obtained from the Beijing Atmospheric Environmental Monitoring Action which was supported by the Beijing Olympic Technological Project (Xin et al., 2010; Gao et al., 2011). Hourly measurements of NO_2, O_3 and $PM_{2.5}$ at seven urban sites shown in Fig. 1 (Li et al., 2011) were used in the analysis.

4. Results and discussion

4.1. Model validation

Previously, the comprehensive model evaluations have been conducted for Case Emis, Case NO_2^* and Case Het (Li et al., 2011; An et al., 2013; Tang et al., 2014). In this section, the simulation results for Case R and Case E are evaluated to examine the performance of the extended WRF-Chem model with the three additional HONO sources. Figure 2 shows the simulations of 24-h average concentrations of HONO, NO_2, NO_3^- and NH_4^+ compared to the measurements conducted at Peking University in Beijing during August 2007. The mean simulated HONO concentration is only 0.08 ppb in Case R. When the additional HONO sources are considered for Case E, the mean HONO concentration is improved up to 1.36 ppb. This value is very close to the observed mean of 1.43 ppb (Fig. 2a). The NO_2 concentrations in Case E are approximately 2–10 ppb lower than those in Case R (Fig. 2b), which is mostly due to the NO_2 heterogeneous reaction on aerosol surfaces. Although the simulated NO_2 agrees reasonably well with most of the observations (Fig. 2b), the simulated NO_3^- overestimates the observations by 5–20% (Fig. 2c) for both Case R and Case E. This NO_3^- overestimation was found in the whole Northeast Asian region (Kajino et al., 2012, 2013) and further investigation with additional observations is required. Both Case R and Case E well reproduce NH_4^+ variations and quantities (Fig. 2d). The correlation coefficient (R) is found as 0.59. The simulated mean NH_4^+ in Cases R and E are 8.55 and 10.27 μg m^{-3}, respectively. The observed mean is 12.27 μg m^{-3}. The additional HONO sources significantly enhanced NO_3^- and NH_4^+ concentrations (Fig. 2c, d), and this resulted in an increase for $PM_{2.5}$ concentrations (An et al., 2013).

The comparison between the simulated and observed hourly concentrations of HONO and OH at the Meteorological Tower in Beijing, NO_2, O_3 and $PM_{2.5}$ at the seven urban sites over the BTH region are shown in the Supplementary file and our previous studies (Li et al., 2011; An et al., 2013; Tang et al., 2014). The simulations generally captured the diurnal variations of pollutants at different sites of the BTH region. The comparative statistics for Case E are given in Table 2. The variations of T, RH, WS and WD near the Meteorological Tower site are generally simulated well. During 13–20 August 2007 the high temperature and humidity values during low speed of southerly wind existed in Beijing. The meteorological conditions as well as the large emissions of NO_x from the heavy traffic (An et al., 2009) nearby the sampling site resulted in the high HONO concentrations. The Case E average predicted HONO concentrations of 1.69 ppb agreed reasonably with the measured concentration of 1.27 ppb. The simulations of Case E also generally captured the hourly variations of NO_2, O_3 and $PM_{2.5}$ at the seven urban sites over the BTH region, with the correlation coefficients being 0.52, 0.87 and 0.51, respectively. The FAC2 (fractions of simulated values within a factor of two of the observed values) for NO_2, O_3 and $PM_{2.5}$ are 0.50, 0.62 and 0.64, respectively (Table 2).

For daytime (7:00–19:00, LT) and night – time (20:00–6:00, LT) conditions, HONO simulations for Case R and

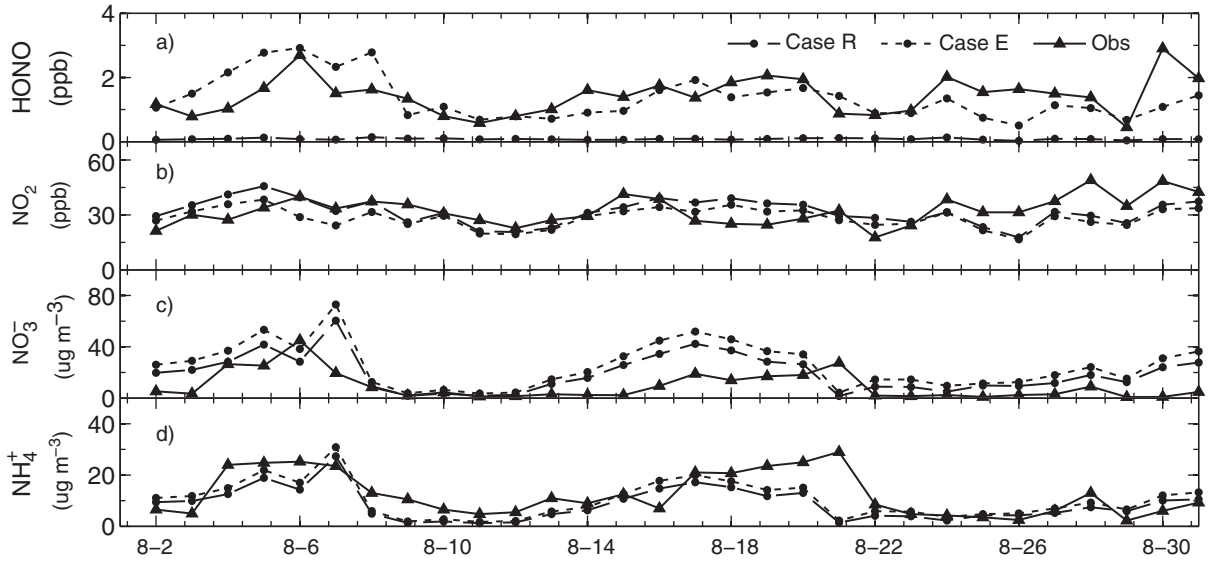

Fig. 2. Comparison of simulated 24-h average (a) HONO, (b) NO_2, (c) NO_3^- and (d) NH_4^+ concentrations with observations at Peking University during August 2007 (Ianniello et al., 2011; Spataro et al., 2013). Case R is a reference case; Case E includes the HONO emissions, NO_2^* chemistry and NO_2 heterogeneous reaction on aerosol surfaces.

Table 2. Statistics for comparison of the observed (Obs.) and simulated (Sim.) hourly data during August 13–20, 2007

	T	RH	WS	WD	HONO	NO_2	O_3	$PM_{2.5}$
Units	°C	%	m s^{-1}	deg	ppb	ppb	ppb	μg m^{-3}
Number of data	184	184	184	184	117	1304	1194	1340
Median (Obs.)	28.00	68.00	1.40	135.0	0.89	17.02	37.23	94.78
Median (Sim.)	29.15	41.11	2.11	190.7	1.49	20.79	32.77	143.86
Mean (Obs.)	28.05	66.45	1.46	136.35	1.27	19.29	44.61	100.11
Mean (Sim.)	28.92	43.29	2.34	185.74	1.69	24.62	38.62	161.18
MB	0.87	−23.15	0.87	49.40	0.42	5.33	−5.99	61.07
NMB[a]	3	−34	52	36	33	28	−13	61
RMSE	1.85	24.78	1.60	133.56	1.05	19.01	18.59	96.84
R	0.94	0.88	0.47	0.42	0.71	0.52	0.87	0.51
FAC2[b]	1.0	0.98	0.55	0.58	0.60	0.50	0.62	0.64

Observations of HONO are from the Beijing Meteorological Tower and the meteorological parameters are from the Olympic Village near to the tower site (see Section 3). NO_2, O_3 and $PM_{2.5}$ measurements are from the seven urban sites over the BTH region (Fig. 1). Model results are for Case E.

[a]The unit of NMB is in %.

[b]Fraction of simulations within a factor of two of observations.

Case E are compared with the observations for the Meteorological Tower (Fig. 3a). The additional HONO sources significantly improved HONO simulations for both daytime and night-time. The simulated mean concentration of HONO for daytime increased from 0.10 ppb in Case R to 0.51 ppb in Case E, and for night-time, it increased from

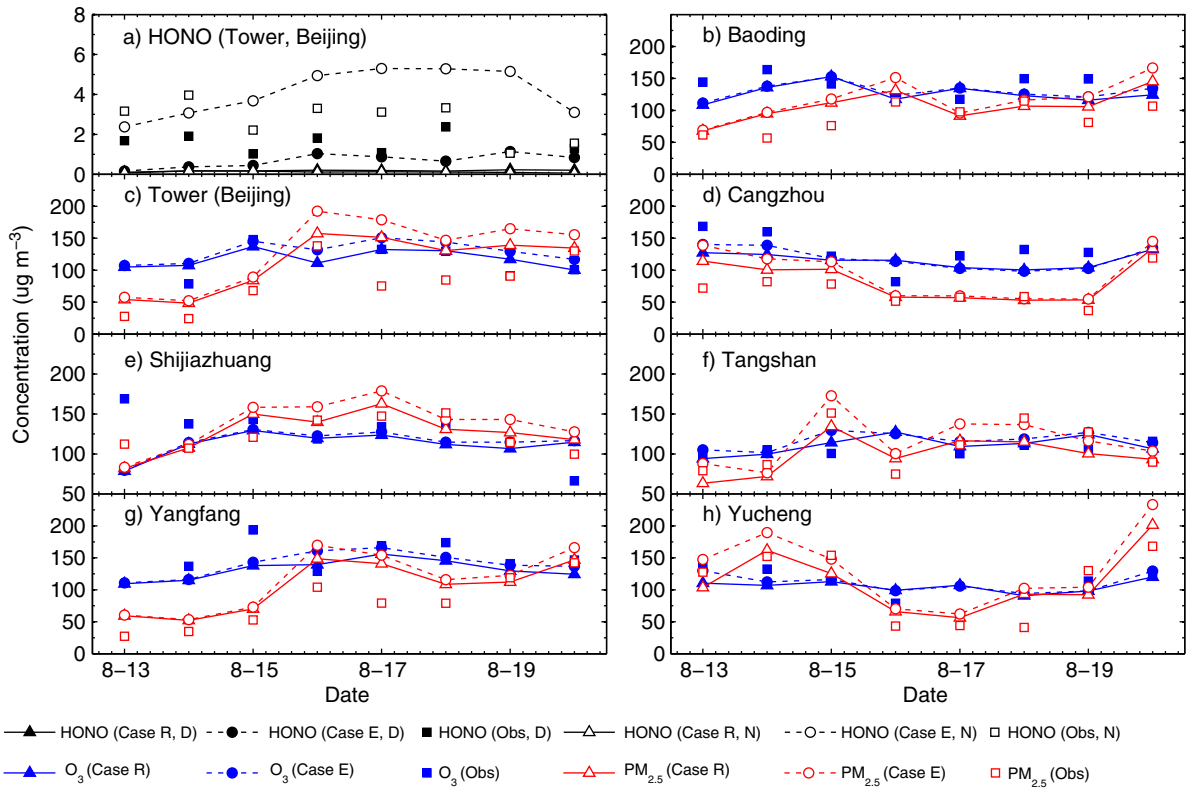

Fig. 3. Observed and simulated (a) daytime (D, 7:00–19:00) and night-time (N, 20:00–6:00) mean concentrations of HONO at the Beijing Meteorological Tower site and (b–h) daytime mean concentrations of O_3 and $PM_{2.5}$ at the seven urban sites over the BTH region during 13–20 August, 2007. The unit used is μg m^{-3} (at 1.01325×10^5 Pa and 25°C, 1 μg m^{-3} is ~0.52 ppb for HONO and ~0.51 ppb for O_3).

0.06 ppb to 2.05 ppb. Figure 3b–h shows the daytime simulations of O_3 and $PM_{2.5}$ at the seven urban sites over the BTH region. Both Cases R and E performed well for predicting O_3 and $PM_{2.5}$ daytime concentrations. The observed and simulated means, the mean bias (MB), the normal mean bias (NMB), the root mean square error (RMSE) and FAC2 of O_3 for Case E are 64.97 ppb, 63.05 ppb, −1.92 ppb, −2.95%, 12.48 ppb, and 0.98, respectively; corresponding $PM_{2.5}$ values for Case E are 94.01 μg m^{-3}, 119.24 μg m^{-3}, 25.23 μg m^{-3}, 26.83%, 36.05 μg m^{-3} and 0.91, respectively.

4.2. *Daytime enhancements of O_3 and $PM_{2.5}$ due to the additional HONO sources*

4.2.1. The chemical coupling between O_3 and $PM_{2.5}$. The chemical coupling between O_3 and $PM_{2.5}$ was emphasised in previous studies (Meng et al., 1997; Nguyen and Dabdub, 2002; Wennberg and Dabdub, 2008). This is of profound importance in understanding processes that control the concentrations of both O_3 and $PM_{2.5}$. As shown in Fig. 4, OH is the essential oxidant during daytime. The OH oxidises VOC to produce O_3 in presence of NO_x and oxidises SO_2 and NO_x to produce secondary inorganic particulate in presence of NH_3. OH and O_3 attack on organic molecules can generate semivolatile secondary organic aerosol (SOA). HONO sources add another level of complexity to this mechanism. When the HONO emissions, NO_2^* chemistry and NO_2 heterogeneous reaction on aerosol surfaces are considered, the OH formation is increased via the HONO photolysis and reaction of NO_2^* with H_2O. The increases in OH concentrations simultaneously enhance O_3 and $PM_{2.5}$

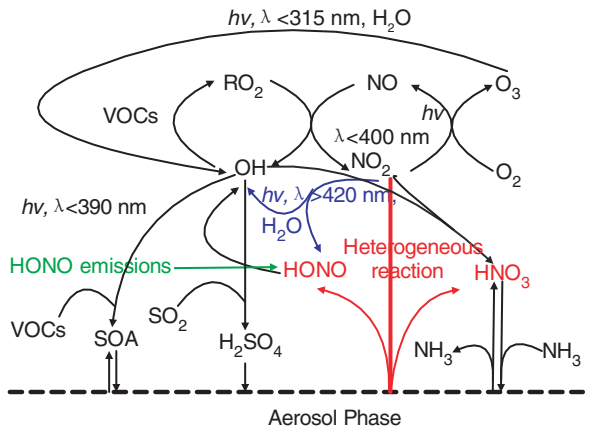

Fig. 4. Impacts of the additional HONO sources on the chemical coupling between ozone and particulate matter. HONO sources increase OH concentrations and subsequently promote O_3 and PM production. HNO_3 produced from the NO_2 heterogeneous reaction on aerosol surfaces enhances nitrate concentrations in presence of NH_3.

production. In addition, increasing O_3 concentration further increases the daytime formation of OH. The OH in turn reacts with NO_2 to form gas nitric acid (HNO_3). The NO_2 heterogeneous reaction on aerosol surfaces also contributes to HNO_3 enhancement, which eventually increases nitrate concentrations.

Although O_3 and $PM_{2.5}$ are subjected to a complex series of common emissions and photochemical production pathways, the coupling between O_3 and $PM_{2.5}$ is in a non-linear manner. O_3 production is related mainly to the VOCs and NO_x gas-phase chemistry while $PM_{2.5}$ production is contributed mostly to the gas-to-particle conversion processes, involving chemical reactions and mass transport in the gas and particle phases (Shiraiwa et al., 2014). The impacts of the additional HONO sources on O_3 and PM enhancements are found to be more significant over urban and coastal areas with high NO_x emissions. On the other hand, the impacts are small in rural and background areas where NO_x emissions are relatively low (Wennberg and Dabdub, 2008; Sarwar et al., 2009; An et al., 2011; Li et al., 2011; Elshorbany et al., 2012, 2014; Jorba et al., 2012; Zhang et al., 2013). In the regions with high VOCs to NO_x ratios (e.g. rural areas), O_3 production is sensitive to NO_x concentrations. The NO_2 reductions due to the NO_2 heterogeneous reaction can decrease O_3 production in rural areas. Therefore, the additional HONO sources are more likely to enhance O_3 and $PM_{2.5}$ simultaneously in urban areas with a low ratio of VOCs to NO_x. In those areas, decreasing NO_2 alone likely leads to increasing O_3 concentrations (Wennberg and Dabdub, 2008; Ensberg et al., 2010).

In order to investigate the impacts of the additional HONO sources on O_3 and $PM_{2.5}$ chemical interactions, the enhancements of daytime mean concentrations of O_3 and $PM_{2.5}$ at the seven urban sites during 13–20 August 2007 shown in Fig. 3 are demonstrated in scatter diagrams (Fig. 5). Both O_3 and $PM_{2.5}$ daytime enhancements (Fig. 5a) due to the NO_2^* chemistry are mostly less than 5 μg m^{-3} (for O_3, 1 μg m^{-3} = 0.51 ppb at 1.01325×10^5 Pa and 25°C). Among the three additional HONO sources, the NO_2 heterogeneous reaction is the largest contributor to O_3 and $PM_{2.5}$ enhancements. Up to 14 μg m^{-3} (7 ppb) and 28 μg m^{-3} increases are found for O_3 and $PM_{2.5}$, respectively (Fig. 5b). The contributions of HONO emissions to O_3 and $PM_{2.5}$ enhancements are relatively small (<2 μg m^{-3}; not shown). The largest enhancements of daytime concentrations of O_3 and $PM_{2.5}$ due to all the three additional HONO sources are estimated to be 17.27 μg m^{-3} (8.79 ppb) for O_3 and 31.54 μg m^{-3} for $PM_{2.5}$ (Fig. 5c). Figure 5 also clearly shows that the daytime O_3 increases are closely related to the daytime $PM_{2.5}$ increases. The correlation coefficients between O_3 and $PM_{2.5}$ enhancements are 0.71 and 0.75, respectively, when the NO_2^* chemistry and NO_2

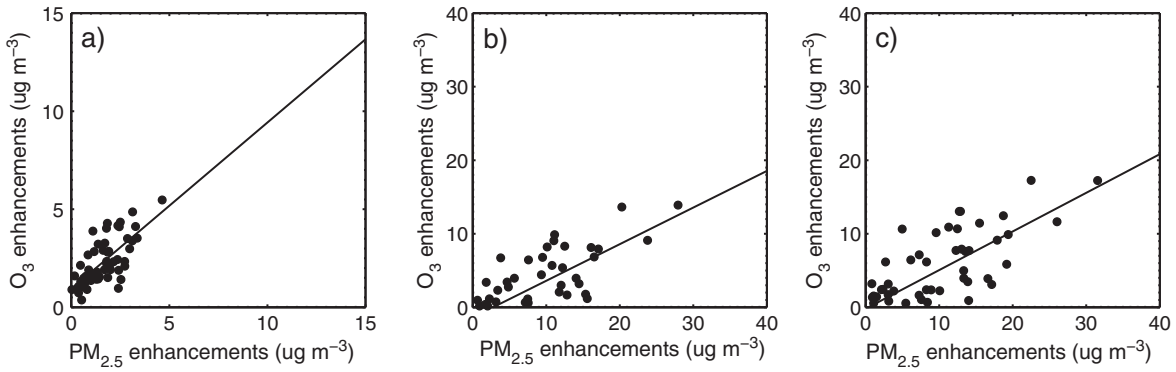

Fig. 5. Enhancements of daytime mean concentrations of O_3 and $PM_{2.5}$ due to (a) the NO_2^* chemistry (b) the NO_2 heterogeneous reaction on aerosols and (c) all the three additional HONO sources at the seven urban sites demonstrated in Fig. 3 during 13–20 August, 2007.

heterogeneous reaction are individually included in the WRF-Chem model.

The correlation coefficient between the daytime enhancement of O_3 and $PM_{2.5}$ over the BTH region for the whole month was estimated. As shown in Fig. 6a, the correlation coefficients between O_3 and $PM_{2.5}$ daytime enhancements due to the additional HONO sources are greater than 0.6 in many urban areas and greater than 0.8 over Beijing and Tianjin areas. The high correlation is found mainly over the urban areas where the values of the linear-fitting slope for O_3 and $PM_{2.5}$ enhancements are above zero (Fig. 6b), indicating that the additional HONO sources increase O_3 and $PM_{2.5}$ concentrations simultaneously. The increases in both O_3 and $PM_{2.5}$ are because of the enhanced OH concentrations as demonstrated in Fig. 4. The significant increases in O_3 concentrations occur in urban areas also

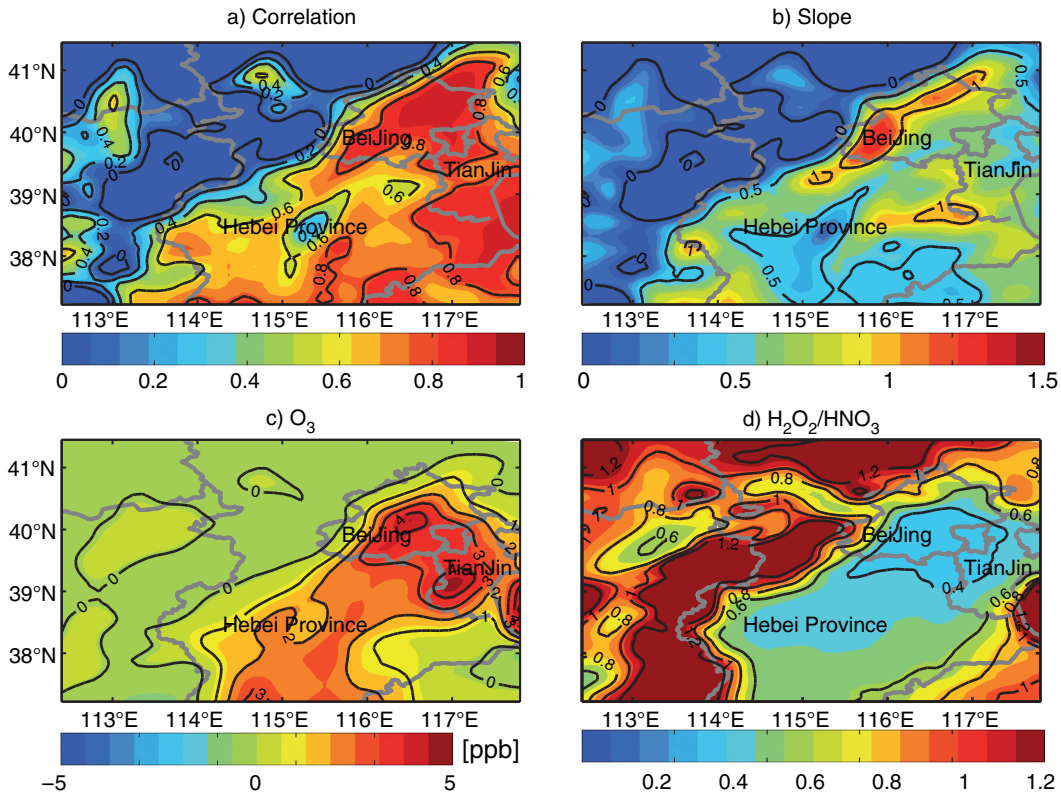

Fig. 6. Values of (a) the correlation coefficient and (b) the linear-fitting slope for O_3 and $PM_{2.5}$ daytime enhancements due to the three additional HONO sources during August 2007; monthly mean daytime (c) O_3 enhancements due to the three additional HONO sources and (d) H_2O_2/HNO_3 ratio over the BTH region.

because O_3 production is mainly sensitive to VOC concentrations in those areas, where the NO_2 decreases due to the NO_2 heterogeneous reaction increase O_3. As shown in Fig. 6c, 2–5 ppb increases in the monthly mean daytime O_3 concentrations are found in Beijing, Tianjin and south of Hebei Province.

The ratio of H_2O_2/HNO_3 is often used as an indicator to identify VOC-sensitive or NO_x-sensitive regimes (Sillman, 1995; Lam et al., 2005). The transition value of 0.4–0.8 is adopted in this study according to the field measurements conducted in Beijing (He et al., 2010): a value < 0.4 indicates a VOC-sensitive regime, a value > 0.8 indicates a NO_x-sensitive regime, and otherwise it indicates an intermediate regime (Fig. 6d). Comparing Fig. 6a and d, it is found that the low correlation (< 0.2) between O_3 and $PM_{2.5}$ daytime enhancements occurs mainly over the rural areas, such as Taihang Mountains to the west of Hebei Province, and Yan Mountains to the north of Beijing. Those rural areas are within the NO_x-sensitive regimes where NO_2 decreases due to the NO_2 heterogeneous reaction (see Fig. 2b and Li et al., 2011) will reduce O_3 (Fig. 6c). Daytime enhancements of O_3 and $PM_{2.5}$ for all the simulated grids within the BTH region during August 2007 are presented in Supplementary Fig. 5. The correlation coefficients between O_3 and $PM_{2.5}$ daytime enhancements are estimated as 0.83, 0.91 and 0.90, for the NO_2^* chemistry, NO_2 heterogeneous reaction and the three additional HONO sources included in the simulations, respectively.

4.2.2. Impacts on concentrations of $PM_{2.5}$ and its major components. The additional HONO sources enhance O_3 production mainly through increasing OH concentrations which will enhance $PM_{2.5}$ production as well. However, the coupling between O_3 and $PM_{2.5}$ production is in a non-linear way. As stated in Fig. 4, $PM_{2.5}$ production also involves complex gas precursors that go through multiphase chemical evolution. Figure 7 shows that the impacts of the additional HONO sources on individual $PM_{2.5}$ components during daytime. NO_3^- has the largest enhancements (10–58%, 4–9 $\mu g\ m^{-3}$), followed by NH_4^+ (10–40%, 1–3 $\mu g\ m^{-3}$) and SO_4^{2-} (5–18%, 0.5–1.5 $\mu g\ m^{-3}$). The large increment is found mainly in areas with high NO_x levels, e.g. Beijing, Tianjin and south of Hebei Province. The HONO-related enhancement of NO_3^- is due to the enhanced OH level (10–40%, Fig. 7e) and the NO_2 heterogeneous reaction that produces more HNO_3 (Fig. 7f). The reason for the enhancement of SO_4^{2-} is that the increasing OH can oxidise SO_2 to produce gas-phase H_2SO_4 and enhance H_2O_2 (Fig. 7g) and O_3 (Fig. 6c), which can oxidise dissolved SO_2 to produce SO_4^{2-} through aqueous phase reactions. The increases in HNO_3 and H_2SO_4 can be neutralised by NH_3 to form NH_4^+. The NO_2 heterogeneous reaction and H_2O_2 enhancements are major reasons for night-time enhancements of $PM_{2.5}$ and its major components (Supplementary Fig. 6) and the contributions of the individual HONO sources to $PM_{2.5}$ and its major inorganic components can be found in An et al. (2013).

Monthly-mean concentrations of $PM_{2.5}$ and its major components characterised by the MOSAIC aerosol module in the WRF-Chem are shown in Supplementary Fig. 7. It should be noted that the formation of SOA is not taken into account in this study. Organic aerosol, especially SOA could contribute significantly to $PM_{2.5}$. In-situ observations showed that OA on average accounted for approximate 40% of submicron aerosols in Beijing during summertime, and SOA dominated OA, contributing 64% (Sun et al., 2012 and references therein). However, the complexity involved in SOA formation makes SOA difficult to be simulated well. Current air quality models have generally underpredicted observed SOA concentrations, with model-measurement discrepancies of a factor of two or more. More recent modelling efforts incorporating a number of additional factors such as new SOA precursors and particle phase chemistry, have begun to close the gap between predicted and measured SOA concentrations. But even for cases when simulations show reasonable agreement with measurements, the agreement may not be for the right reasons (Hallquist et al., 2009). The impacts of the additional HONO sources on SOA concentrations will be considered in following studies since the enhancement of the oxidants augments the production of semi-VOCs, which are apt to partition more to particle phase and further escalates the SOA concentrations (Li et al., 2010).

4.3. Sensitivity of O_3 and $PM_{2.5}$ to the additional HONO sources

Impacts of the additional HONO sources on the O_3 and $PM_{2.5}$ chemical coupling require rethinking of their control strategies. Meng et al. (1997) suggested that attempts to reduce PM levels required control of the NO_x and VOC emissions that are also precursors to O_3 formation. The O_3 control strategies rely primarily on NO_x and VOC emission variations. The urban areas of Beijing are often in a VOC-sensitive regime for ozone chemistry (see Fig. 6d and Wang et al., 2006). This section mainly presents the simulation results for Beijing Meteorological Tower, where the traffic emissions are large (An et al., 2009).

The resulting peak 8-h average ozone isopleths are shown in Fig. 8. Figure 8a shows that with decreased VOC emissions, $O_{3\_8h;max}$ concentrations are reduced steadily, whereas a decrease in NO_x emissions over 50% is necessary to obtain the O_3 reduction. Figure 8b shows the differences in $O_{3\_8h;max}$ concentrations between Cases E and R.

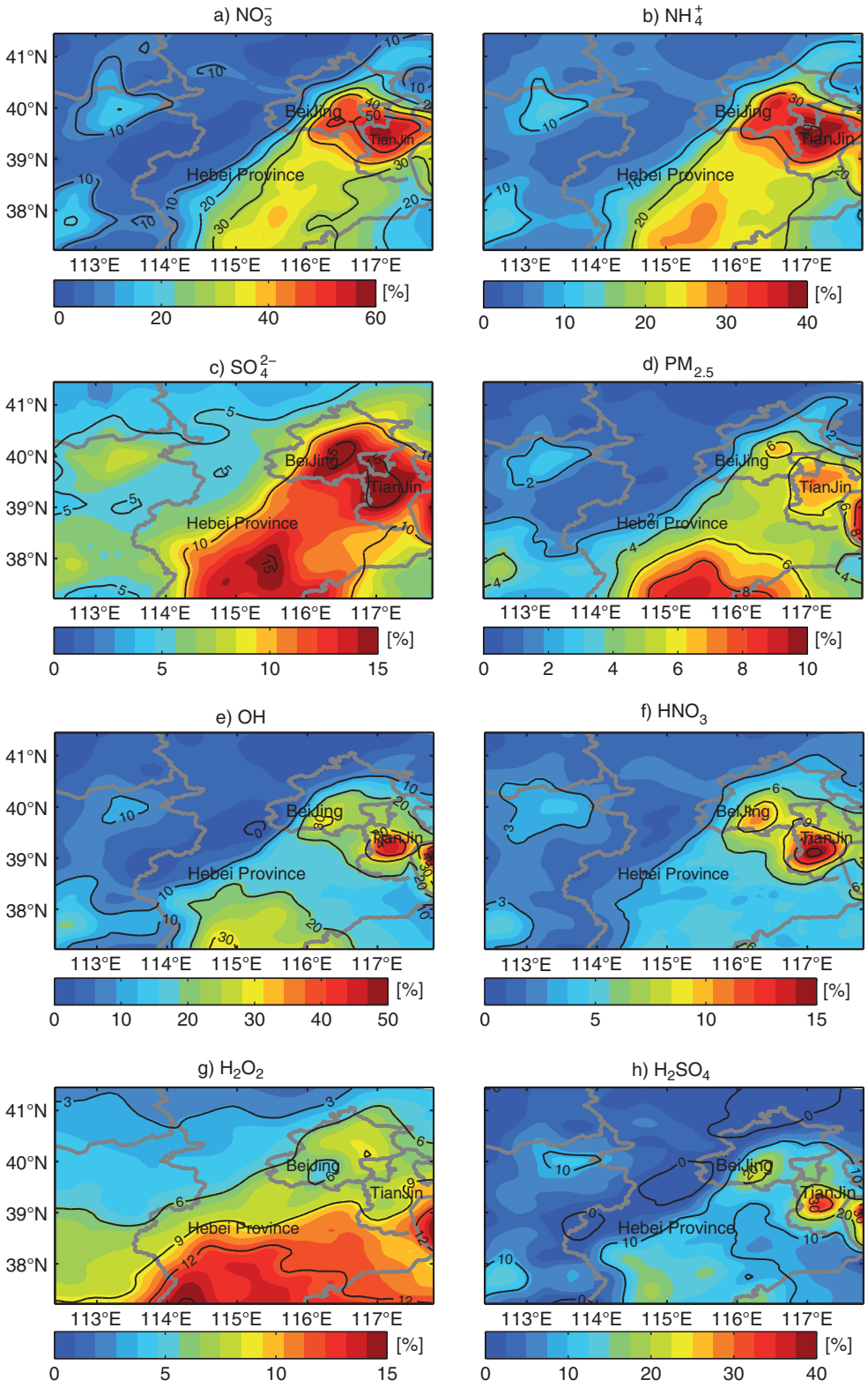

Fig. 7. Percentage increases of monthly-mean daytime (a) NO_3^-, (b) NH_4^+ and (c) SO_4^{2-} in $PM_{2.5}$ and (d) $PM_{2.5}$, (e) OH, (f) HNO_3, (g) H_2O_2 and (h) H_2SO_4 concentrations over the BTH region during August 2007 due to the three additional HONO sources.

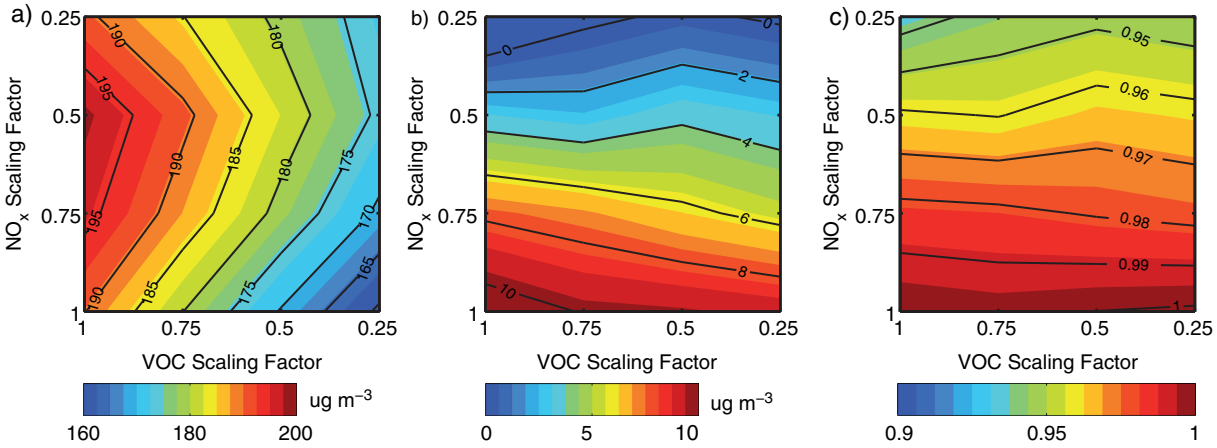

Fig. 8. Impacts of the additional HONO sources on $O_{3\_8h;max}$ concentrations resulting from the control of NO_x, VOC and NH_3 emissions. (a) $O_{3\_8h;max}$ concentrations for Case R in Beijing on 17 August 2007; (b) $O_{3\_8h;max}$ concentrations for Case E minus those for Case R; (c) ratio of Relative Reduction Factors (RRF) for Case E divided by RRF for Case R.

The additional HONO sources increase $O_{3\_8h;max}$ concentrations but the enhancements decline as NO_x emissions decrease, indicating that the impacts of the additional HONO sources on O_3 are significant in areas with high NO_x emissions (Sarwar et al., 2009; Ensberg et al., 2010).

In regulatory applications, the relative reduction factors (RRF) can be used to reflect control strategy effectiveness. RRF for a given pair of VOCs and NO_x reduction factors, RRF (f_{VOC}, f_{NOx}), are calculated as the ratio of $O_{3\_8h;max}$ resulting from that particular pair (f_{VOC}, f_{NOx}) divided by $O_{3\_8h;max}$ from $f_{VOC} = 1.0$ and $f_{NOx} = 1.0$ (Hogrefe et al., 2008). Figure 8c presents the ratio of the RRF obtained in Case E divided by that obtained in Case R. The RRF ratios are below one under nearly all control scenarios, illustrating that the enhanced HONO sources increase the effectiveness of the control strategies in reducing O_3 concentrations, especially through NO_x emission decreases. For example, when the additional HONO sources are considered, a reduction of 75% in emitted NO_x leads to an O_3 reduction of 6.5% more than the O_3 reduction obtained in a case without the additional HONO sources. The RRF in Case E is up to 7% lower than that in Case R, similar to the results obtained in Los Angeles where the NO_2^* chemistry produced RRF 5% lower than that in the reference case (Ensberg et al., 2010).

The additional HONO sources also affect $PM_{2.5}$ control strategies. Figure 9 shows isopleths of the 24-h average concentrations of $PM_{2.5}$ for Cases R and E. Although $PM_{2.5}$ decreases with any reductions of NO_x, VOCs or NH_3 emissions in both cases, the additional HONO sources induce more reductions of $PM_{2.5}$ in Case E than those in Case R. For example, when the NO_x reduction factor declines from 1 to 0.25, $PM_{2.5}$ is decreased from 143.1 μg m^{-3} to 123.8 μg m^{-3}, with a reduction of 13.5% in Case R (Fig. 9a), whereas $PM_{2.5}$ is decreased from 163.1 μg m^{-3} to 128.6 μg m^{-3}, with a reduction of 21.1% in Case E (Fig. 9d).

The present results are found to be in agreement with previous studies. Ensberg et al. (2010) showed that the NO_2^* chemistry increases the sensitivity of particle formation to changes in NO_x emissions. In addition, the results in this study show that the three additional HONO sources also increase the sensitivity of $PM_{2.5}$ formation to changes in NH_3 emissions. Comparing Fig. 9b and e, the number of isopleths in Case E is more than that in Case R as NH_3 emissions are reduced, indicating that a decrease in NH_3 emissions leads to more $PM_{2.5}$ reduction in Case E than that in Case R. Figure 9c and f show that reducing NO_x and NH_3 emissions simultaneously results in significant decreases in $PM_{2.5}$ concentrations. When NO_x and NH_3 reduction factors decrease from 1 to 0.25, the $PM_{2.5}$ reduction in Case E is found to be 8% larger than that in Case R.

To better understand the effects of the additional HONO sources on $PM_{2.5}$ and O_3 control strategies, Fig. 10 illustrates how many times the concentration reductions of $PM_{2.5}$ and O_3 fall in a certain range due to the emission reductions of NO_x, VOCs and NH_3. Among the 64 sensitivity simulations (see Section 2.2), the number of large reductions of $PM_{2.5}$ or O_3 in Case E is more than that in Case R. For example, the number of $PM_{2.5}$ reductions in the range of −25 to −20% is 17 in Case E, whereas that in Case R is 4. The number of O_3 reductions in the range of −15 to −10% is 20 in Case E, much larger than that of 8 in Case R. Figure 11 further shows that within the same range of $PM_{2.5}$ or O_3 reductions in Cases R and E, the frequency of large decreases in pollutant emissions is much

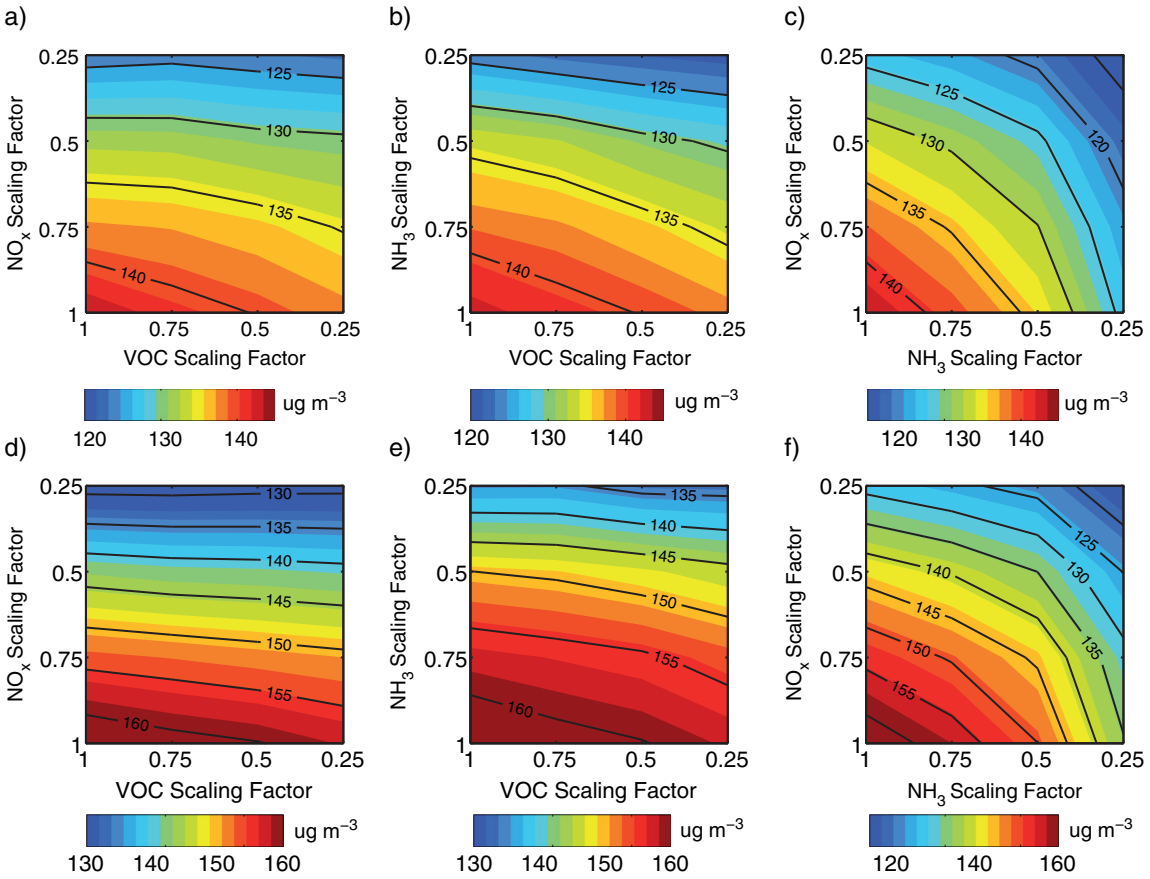

Fig. 9. Twenty four-hour average $PM_{2.5}$ concentrations for Case R (a–c) and for Case E (d–f) in Beijing on 17 August 2007.

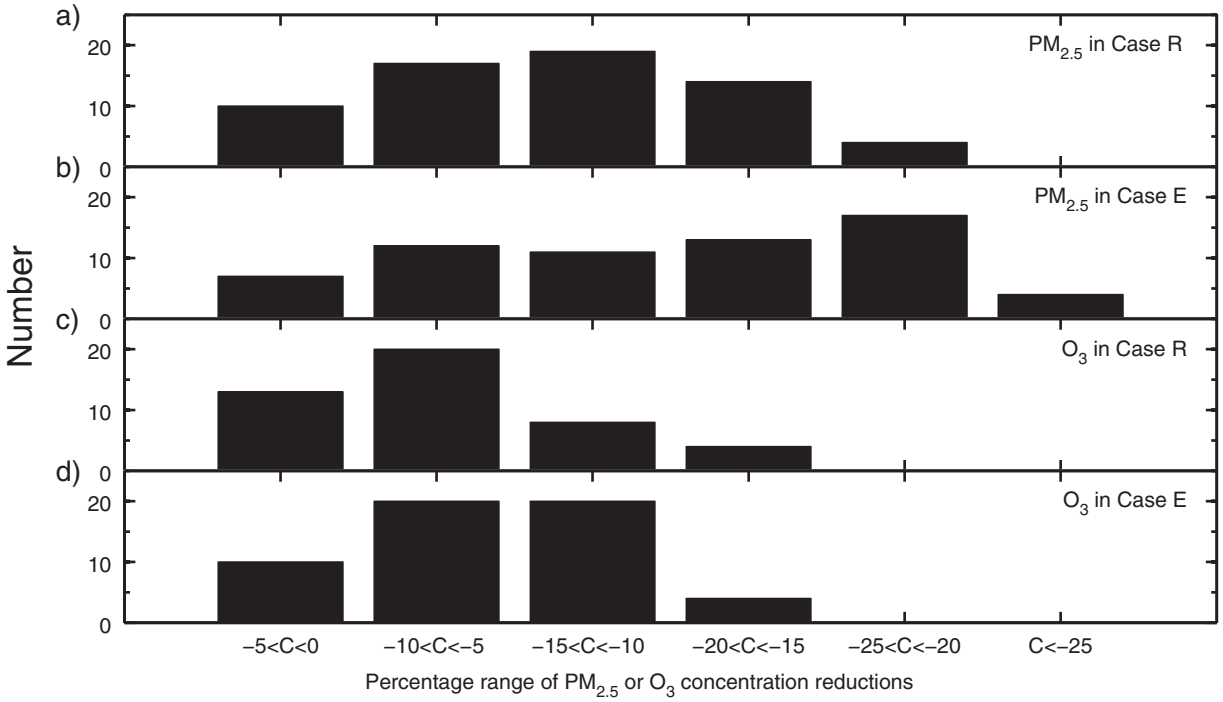

Fig. 10. The number of concentration reductions (C, with unit of %) of (a) $PM_{2.5}$ in Case R, (b) $PM_{2.5}$ in Case E, (c) O_3 in Case R, and (d) O_3 in Case E in a certain reduction range among the sensitivity simulations using the 64 emission scenarios (see Section 2.2).

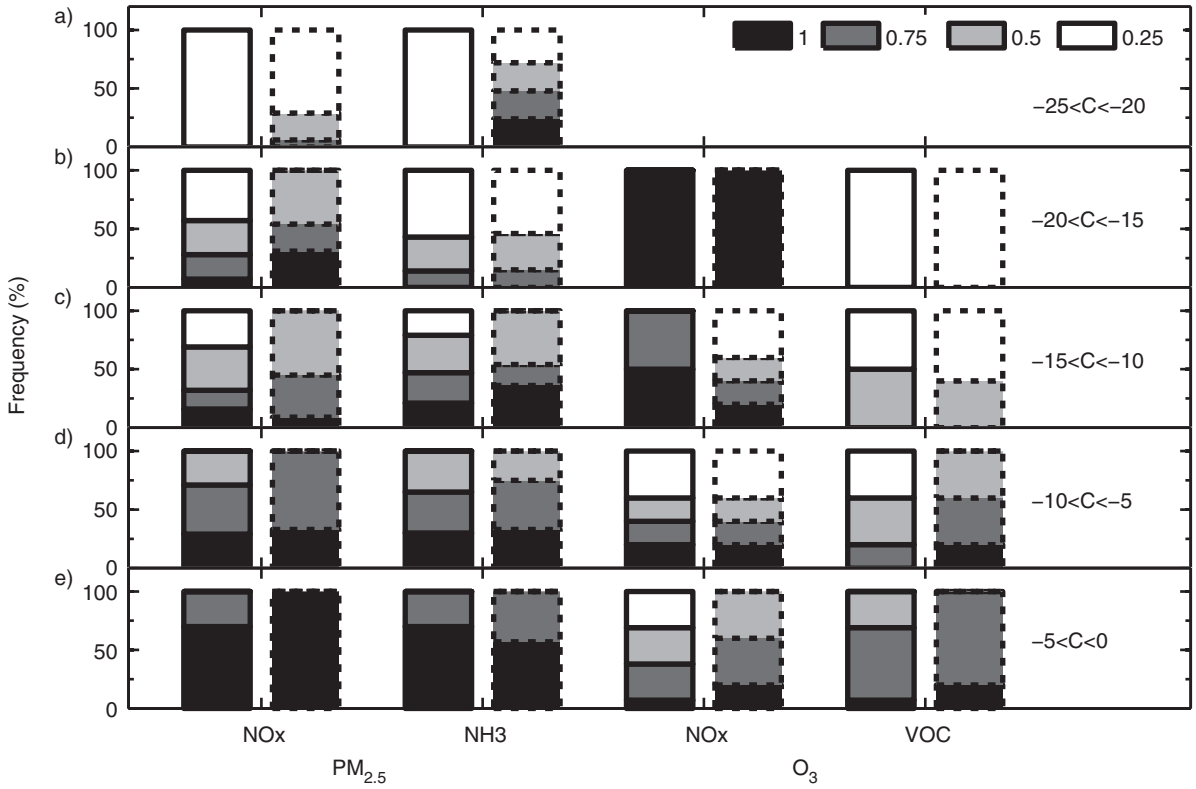

Fig. 11. Comparison of NO_x, VOC and NH_3 emission reductions between Case R (bars with solid baselines) and Case E (bars with dotted baselines) to gain the same range of $PM_{2.5}$ or O_3 concentration reductions (C, in unit of %) of (a) $-25\% < C < -20\%$; (b) $-20\% < C < -15\%$; (c) $-15\% < C < -10\%$; (d) $-10\% < C < -5\%$; and (e) $-5\% < C < 0$. The frequency for each scaling factor is computed by T_i/T, where T is the total times for $PM_{2.5}$ or O_3 concentration reductions falling in a certain reduction range; T_i is the occurrence times within T for a specific scaling factor (1, 0.75, 0.5 or 0.25 shown in Section 2.2).

less in Case E than that in Case R. For example, the frequency of NO_x, VOC and NH_3 reduction factors of 0.25 is less in Case E than that in Case R in a certain range of $PM_{2.5}$ or O_3 concentration reductions. The frequency of 50% decreases in NO_x and NH_3 emissions in Case E for the $PM_{2.5}$ reductions between -10 and -5% is also much smaller than that in Case R (Fig. 11d). These results further indicate that the additional HONO sources enhance the effectiveness of control strategies for reducing $PM_{2.5}$ and O_3 concentrations.

5. Conclusions

Three additional HONO sources, i.e. the HONO emissions, NO_2^* chemistry and NO_2 heterogeneous reaction on aerosol surfaces, were added into a fully coupled meteorology–chemistry model called WRF-Chem to examine how the additional HONO sources influence O_3 and $PM_{2.5}$ chemical coupling and their control strategies. The following main conclusions are obtained from the current study:

(1) The three additional HONO sources significantly increased daytime O_3 and $PM_{2.5}$ concentrations over the urban areas of the BTH region. The enhancements of up to 9 ppb for O_3 and 32 μg m^{-3} for $PM_{2.5}$ are found at the seven urban sites during August 2007. The NO_2 heterogeneous reaction on aerosol surfaces is the largest contributor to the enhancements of O_3 and $PM_{2.5}$ during daytime.

(2) The O_3 increases are found to be closely associated with $PM_{2.5}$ increases over VOC-sensitive regimes during daytime when the additional HONO sources are considered. The correlation coefficient between O_3 and $PM_{2.5}$ daytime enhancements is estimated to be greater than 0.6 in many urban areas of the BTH region and > 0.8 over Beijing and Tianjin areas.

(3) The additional HONO sources enhance $PM_{2.5}$ components of SO_4^{2-}, NO_3^- and NH_4^+, which are increased by 5–18, 10–58 and 10–40%, respectively, over urban areas during daytime. The simultaneous increment of O_3 and $PM_{2.5}$ during daytime due to the additional HONO sources is related to the increasing oxidants (OH, H_2O_2 and O_3) that enhance the atmospheric oxidising capacity. The 20–40%

enhancements of the monthly mean daytime OH concentrations are found over Beijing, Tianjin and south of Hebei Province.

(4) The changes in O_3 and $PM_{2.5}$ concentrations under a variety of NO_x, VOC and NH_3 emission reduction scenarios revealed that the additional HONO sources enhanced the effectiveness of control strategies for reducing O_3 and $PM_{2.5}$ concentrations.

(5) A decrease in NO_x emissions produced more decreases in O_3 concentrations when the additional HONO sources were included. The additional HONO sources resulted in the O_3 RRF 7% lower than that in the reference case and this is consistent with the recent study conducted for the South Coast Air Basin of California (Ensberg et al., 2010).

(6) The additional HONO sources significantly increased $PM_{2.5}$ sensitivity to the changes in NO_x and NH_3 emissions.

The results presented in this study suggest that the complex chemical interactions between O_3 and $PM_{2.5}$ need better explanations when the additional HONO sources are considered. Without considering the additional HONO sources, the effectiveness of emission control strategies in reducing O_3 and $PM_{2.5}$ concentrations would be underestimated significantly. The effects of HONO sources on SOA concentrations will be evaluated in the following studies.

6. Acknowledgements

The research was partly supported by the National Natural Science Foundation of China (Grant No. 41405121 and 41175105), the Beijing Municipal Natural Science Foundation (Grant No. 8144054), the Key Project of Chinese Academy of Sciences (XDB05030301), and the Carbon and Nitrogen Cycle project of Institute of Atmospheric Physics, Chinese Academy of Sciences. Special thanks are given to Prof. Pinhua Xie from Anhui Institute of Optics and Fine Mechanics, Chinese Academy of Sciences for providing hourly HONO observations in Beijing and Dr. Bo Hu and Dongsheng Ji from the Chinese Ecosystem Research Network (CERN). NO_2, O_3 and $PM_{2.5}$ observed data at seven sites over the BTH region were obtained from the CERN.

References

Alicke, B., Platt, U. and Stutz, J. 2002. Impact of nitrous acid photolysis on the total hydroxyl radical budget during the Limitation of Oxidant Production/Pianura Padana Produzione di Ozono study in Milan. *J. Geophys. Res.* **107**(D22), 8196. DOI: 10.1029/2000JD000075.

Amedro, D., Parker, A. E., Schoemaecker, C. and Fittschen, C. 2011. Direct observation of OH radicals after 565 nm multi-photon excitation of NO_2 in the presence of H_2O. *Chem. Phys. Lett.* **513**, 12–16.

An, J., Li, Y., Chen, Y., Li, J., Qu, Y. and co-author. 2013. Enhancements of major aerosol components due to three HONO sources in the North China Plain (NCP) and implications for visibility and haze. *Adv. Atmos. Sci.* **30**(1), 57–66.

An, J., Li, Y., Wang, F. and Xie, P. 2011. Impacts of photoexcited NO_2 chemistry and heterogeneous reactions on concentrations of O_3 and NO_y in Beijing, Tianjin and Hebei Province of China. In: *Air Quality-Models and Applications* (ed. N. Mazzeo). InTech, Rijeka, pp. 197–210.

An, J., Zhang, W. and Qu, Y. 2009. Impacts of a strong cold front on concentrations of HONO, HCHO, O_3, and NO_2 in the heavy traffic urban area of Beijing. *Atmos. Environ.* **43**, 3454–3459.

Carr, S., Heard, D. and Blitz, M. 2009. Comment on "Atmospheric hydroxyl radical production from electronically excited NO_2 and H_2O". *Science* **324**(5925), 336.

Chan, C. K. and Yao, X. 2008. Air pollution in mega cities in China. *Atmos. Environ.* **42**(1), 1–42.

Crowley, J. N. and Carl, S. A. 1997. OH formation in the photoexcitation of NO_2 beyond the dissociation threshold in the presence of water vapor. *J. Phys. Chem. A.* **101**(23), 4178–4184.

Elshorbany, Y. F., Crutzen, P. J., Steil, B., Pozzer, A., Tost, H. and co-author. 2014. Global and regional impacts of HONO on the chemical composition of clouds and aerosols. *Atmos. Chem. Phys.* **14**, 1167–1184.

Elshorbany, Y. F., Steil, B., Brühl, C. and Lelieveld, J. 2012. Impact of HONO on global atmospheric chemistry calculated with an empirical parameterization in the EMAC model. *Atmos. Chem. Phys.* **12**, 9977–10000.

Emmons, L., Walters, S., Hess, P., Lamarque, J., Pfister, G. and co-authors. 2010. Description and evaluation of the Model for Ozone and Related chemical Tracers, version 4 (MOZART-4). *Geosci. Model Dev.* **3**, 43–67.

Ensberg, J. J., Carreras-Sospedra, M. and Dabdub, D. 2010. Impacts of electronically photo-excited NO_2 on air pollution in the South Coast Air Basin of California. *Atmos. Chem. Phys.* **10**, 1171–1181.

Fast, J. D., Gustafson, W. I. Jr., Easter, R. C., Zaveri, R. A., Barnard, J. C. and co-authors. 2006. Evolution of ozone, particulates, and aerosol direct radiative forcing in the vicinity of Houston using a fully coupled meteorology-chemistry-aerosol model. *J. Geophys. Res.* **111**, D21305. DOI: 10.1029/2005JD006721.

Finlayson-Pitts, B., Wingen, L., Sumner, A., Syomin, D. and Ramazan, K. 2003. The heterogeneous hydrolysis of NO_2 in laboratory systems and in outdoor and indoor atmospheres: an integrated mechanism. *Phys. Chem. Chem. Phys.* **5**(2), 223–242.

Foley, K., Roselle, S., Appel, K., Bhave, P., Pleim, J. and co-authors. 2010. Incremental testing of the Community Multiscale Air Quality (CMAQ) modeling system version 4.7. *Geosci. Model Dev.* **3**(1), 205–226.

Gao, Y., Liu, X., Zhao, C. and Zhang, M. 2011. Emission controls versus meteorological conditions in determining aerosol concentrations in Beijing during the 2008 Olympic Games. *Atmos. Chem. Phys.* **11**, 12437–12451.

Grell, G. A., Peckham, S. E., Schmitz, R., McKeen, S. A., Frost, G. and co-authors. 2005. Fully coupled "online" chemistry within the WRF model. *Atmos. Environ.* **39**, 6957–6975.

Guenther, A. B., Zimmerman, P. R., Harley, P. C., Monson, R. K. and Fall, R. 1993. Isoprene and monoterpene emission rate variability: model evaluations and sensitivity analyses. *J. Geophys. Res.* **98**(D7), 12609–12617.

Gutzwiller, L., Arens, F., Baltensperger, U., Gaggeler, H. W. and Ammann, M. 2002. Significance of semivolatile diesel exhaust organics for secondary HONO formation. *Environ. Sci. Technol.* **36**(4), 677–682.

Hallquist, M., Wenger, J., Baltensperger, U., Rudich, Y., Simpson, D. and co-authors. 2009. The formation, properties and impact of secondary organic aerosol: current and emerging issues. *Atmos. Chem. Phys.* **9**, 5155–5236.

He, S. Z., Chen, Z. M., Zhang, X., Zhao, Y., Huang, D. M. and co-authors. 2010. Measurement of atmospheric hydrogen peroxide and organic peroxides in Beijing before and during the 2008 Olympic Games: chemical and physical factors influencing their concentrations. *J. Geophys. Res.* **115**, D17307. DOI: 10.1029/2009JD13544.

Hogrefe, C., Civerolo, K. L., Hao, W., Ku, J. Y., Zalewsky, E. E. and co-author. 2008. Rethinking the assessment of photochemical modeling systems in air quality planning applications. *J. Air Waste Manage. Assoc.* **58**(8), 1086–1099.

Ianniello, A., Spataro, F., Esposito, G., Allegrini, I., Hu, M. and co-author. 2011. Chemical characteristics of inorganic ammonium salts in $PM_{2.5}$ in the atmosphere of Beijing (China). *Atmos. Chem. Phys.* **11**, 10803–10822.

Jacob, D. J. 2000. Heterogeneous chemistry and tropospheric ozone. *Atmos. Environ.* **34**, 2131–2159.

Jenkin, M., Utembe, S. and Derwent, R. 2008. Modelling the impact of elevated primary NO_2 and HONO emissions on regional scale oxidant formation in the UK. *Atmos. Environ.* **42**(2), 323–336.

Jenkin, M. E., Cox, R. A. and Williams, D. J. 1988. Laboratory studies of the kinetics of formation of nitrous acid from the thermal reaction of nitrogen dioxide and water vapour. *Atmos. Environ.* (1967) **22**(3), 487–498.

Jorba, O., Dabdub, D., Blaszczak-Boxe, C., Pérez, C., Janjic, Z. and co-authors. 2012. Potential significance of photoexcited NO_2 on global air quality with the NMMB/BSC chemical transport model. *J. Geophys. Res.* **117**, D13301. DOI: 10.1029/2012JD017730.

Kajino, M., Inomata, Y., Sato, K., Ueda, H., Han, Z. and co-authors. 2012. Development of an aerosol chemical transport model RAQM2 and predications of Northeast Asian aerosol mass, size, chemistry, and missing type. *Atmos. Chem. Phys.* **12**, 11833–11856.

Kajino, M., Sato, K., Inomata, Y. and Ueda, H. 2013. Source-receptor relationships of nitrate in Northeast Asia and influence of sea salt on the long-range transport of nitrate. *Atmos. Environ.* **79**, 67–78.

Kleffmann, J., Becker, K. and Wiesen, P. 1998. Heterogeneous NO_2 conversion processes on acid surfaces: possible atmospheric implications. *Atmos. Environ.* **32**(16), 2721–2729.

Kleffmann, J., Gavriloaiei, T., Hofzumahaus, A., Holland, F., Koppmann, R. and co-authors. 2005. Daytime formation of nitrous acid: a major source of OH radicals in a forest. *Geophys. Res. Lett.* **32**, L05818. DOI: 10.1029/2005GL022524.

Kurtenbach, R., Becker, K. H., Gomes, J. A. G., Kleffmann, J., Lörzer, J. C. and co-authors. 2001. Investigations of emissions and heterogeneous formation of HONO in a road traffic tunnel. *Atmos. Environ.* **35**, 3385–3394.

Lam, K. S., Wang, T. J., Wu, C. L. and Li, Y. S. 2005. Study on an ozone episode in hot season in Hong Kong and transboundary air pollution over Pearl River Delta region of China. *Atmos. Environ.* **39**, 1967–1977.

Li, G., Lei, W., Zavala, M., Volkamer, R., Dusanter, S. and co-authors. 2010. Impacts of HONO sources on the photochemistry in Mexico City during the MCMA-2006/MILAGO Campaign. *Atmos. Chem. Phys.* **10**, 6551–6567.

Li, S., Matthews, J. and Sinha, A. 2008. Atmospheric hydroxyl radical production from electronically excited NO_2 and H_2O. *Science* **319**, 1657–1660.

Li, Y., An, J. and Gultepe, I. 2014. Effects of additional HONO sources on visibility over the North China Plain. *Adv. Atmos. Sci.* **31**(5), 1221–1232.

Li, Y., An, J., Min, M., Zhang, W., Wang, F. and co-author. 2011. Impacts of HONO sources on the air quality in Beijing, Tianjin and Hebei Province of China. *Atmos. Environ.* **45**(27), 4735–4744.

Meng, Z., Dabdub, D. and Seinfeld, J. H. 1997. Chemical coupling between atmospheric ozone and particulate matter. *Science* **277**, 116–119.

Nguyen, K. and Dabdub, D. 2002. NO_x and VOC control and its effects on the formation of aerosols. *Aerosol Sci. Tech.* **36**(5), 560–572.

Oswald, R., Behrendt, T., Ermel, M., Wu, D., Su, H. and co-author. 2013. HONO emissions from soil bacteria as a major source of atmospheric reactive nitrogen. *Science* **341**, 1233–1235.

Sarwar, G., Pinder, R. W., Appel, K. W., Mathur, R. and Carlton, A. G. 2009. Examination of the impact of photoexcited NO_2 chemistry on regional air quality. *Atmos. Environ.* **43**, 6383–6387.

Sarwar, G., Roselle, S. J., Mathur, R., Appel, W., Dennis, R. L. and co-author. 2008. A comparison of CMAQ HONO predictions with observations from the Northeast Oxidant and Particle Study. *Atmos. Environ.* **42**(23), 5760–5770.

Shiraiwa, M., Berkemeier, T., Schilling-Fahnestock, K.A., Seinfeld, J.H. and Pöschl, U. 2014. Molecular corridors and kinetic regimes in the multiphase chemical evolution of secondary organic aerosol. *Atmos. Chem. Phys.* **14**, 1–19.

Sillman, S. 1995. The use of NO_y, H_2O_2, and HNO_3 as indicators for ozone-NO_x-hydrocarbon sensitivity in urban locations. *J. Geophys. Res.* **100**(D7), 14175–14188.

Simpson, D., Guenther, A., Hewitt, C. N. and Steinbrecher, R. 1995. Biogenic emissions in Europe: 1. Estimates and uncertainties. *J. Geophys. Res.* **100**(D11), 22875–22890.

Spataro, F., Ianniello, A., Esposito, G., Allegrini, I., Zhu, T. and co-author. 2013. Occurrence of atmospheric nitrous acid in the urban area of Beijing (China). *Sci. Total Environ.* **447**, 210–224.

Sun, Y., Wang, Z., Dong, H., Yang, T., Li, J. and co-authors. 2012. Characterization of summer organic and inorganic aerosols in Beijing, China with an aerosol chemical speciation monitor. *Atmos. Environ.* **51**, 250–259.

Sun, Y., Wang, Z., Fu, P., Yang, T., Jiang, Q. and co-authors. 2013. Aerosol composition, sources and processes during wintertime in Beijing, China. *Atmos. Chem. Phys.* **13**(9), 4577–4592.

Tang, Y., An, J., Li, Y. and Wang, F. 2014. Uncertainty in the uptake coefficient for HONO formation on soot and its impacts on concentrations of major chemical components in the Beijing-Tianjin-Hebei region. *Atmos. Environ.* **84**, 163–171.

Wang, T., Ding, A., Gao, J. and Wu, W. S. 2006. Strong ozone production in urban plumes from Beijing, China. *Geophys. Res. Lett.* **33**, L21806. DOI: 10.1029/2006GL027689.

Wennberg, P. O. and Dabdub, D. 2008. Rethinking ozone production. *Science* **319**, 1624–1625.

Wu, N. and Chen, X. 2012. Two photon dissociation dynamics of NO_2 and NO_2+H_2O. *J. Phys. Chem. C* **116**(25), 6894–6900.

Xin, J., Wang, Y., Tang, G., Wang, L., Sun, Y. and co-author. 2010. Variability and reduction of atmospheric pollutants in Beijing and its surrounding area during the Beijing 2008 Olympic Games. *Chinese Sci. Bull.* **55**(18), 1937–1944.

Zaveri, R. A., Easter, R. C., Fast, J. D. and Peters, L. K. 2008. Model for simulating aerosol interactions and chemistry (MOSAIC). *J. Geophys. Res.* **113**, D13204. DOI: 10.1029/2007JD008782.

Zaveri, R. A. and Peters, L. K. 1999. A new lumped structure photochemical mechanism for large-scale applications. *J. Geophys. Res.* **104**, D23, 30387–30415.

Zhang, Q., Streets, D. G., Carmichael, G. R., He, K. B., Huo, H. and co-authors. 2009. Asian emissions in 2006 for the NASA INTEX-B mission. *Atmos. Chem. Phys.* **9**, 5131–5153.

Zhang, R., Sarwar, G., Fung, J. C. H. and Lau, A. K. H. 2013. Role of photoexcited nitrogen dioxide chemistry on ozone formation and emission control strategy over the Pearl River Delta, China. *Atmos. Res.* **132–133**, 332–344.

Zhao, X., Zhao, P., Xu, J., Meng, W., Pu, W. and co-authors. 2013. Analysis of a winter regional haze event and its formation mechanism in the North China Plain. *Atmos. Chem. Phys.* **13**(11), 5685–5696.

Zhu, Y., Hiu, W., Xie, P., Dou, K., Liu, S. and co-authors. 2009. Observational study of atmospheric HONO in summer of Beijing. *Environ. Sc.* **30**(6), 1567–1573. (in Chinese)